Published in final edited form as:
ACS Chem Biol. 2011 August 19; 6(8): 845–856. doi:10.1021/cb200146a.

Selective inhibition of the $K_{ir}2$ family of inward rectifier potassium channels by a small molecule probe: the discovery, SAR and pharmacological characterization of ML133

Hao-Ran Wang[1,†], **Meng Wu**[1,†], **Haibo Yu**[1], **Shunyou Long**[1], **Amy Stevens**[1], **Darren W. Engers**[2], **Henry Sackin**[3], **J. Scott Daniels**[2], **Eric S. Dawson**[2], **Corey R. Hopkins**[2], **Craig W. Lindsley**[2,*], **Min Li**[1,*], and **Owen B McManus**[1]

[1]Department of Neuroscience, High Throughput Biology Center and Johns Hopkins Ion Channel Center, School of Medicine, Johns Hopkins University, 733 North Broadway, Baltimore, MD 21205

[2]Vanderbilt Specialized Chemistry Center, Department of Pharmacology, Vanderbilt Center for Neuroscience Drug Discovery, Vanderbilt University Medical Center, Nashville, TN 37232

[3]Department of Physiology and Biophysics, Rosalind Franklin University of Medicine and Science, North Chicago, IL

Abstract

The K_{ir} inward rectifying potassium channels have a broad tissue distribution and are implicated in a variety of functional roles. At least seven classes ($K_{ir}1 – K_{ir}7$) of structurally related inward rectifier potassium channels are known, and there are no selective small molecule tools to study their function. In an effort to develop selective $K_{ir}2.1$ inhibitors, we performed a high-throughput screen (HTS) of more than 300,000 small molecules within the MLPCN for modulators of $K_{ir}2.1$ function. Here we report one potent $K_{ir}2.1$ inhibitor, ML133, which inhibits $K_{ir}2.1$ with IC_{50} of 1.8 μM at pH 7.4 and 290 nM at pH 8.5, but exhibits little selectivity against other members of Kir2.x family channels. However, ML133 has no effect on $K_{ir}1.1$ (IC_{50} > 300 μM), and displays weak activity for $K_{ir}4.1$ (76 μM) and $K_{ir}7.1$ (33 μM), making ML133 the most selective small molecule inhibitor of the K_{ir} family reported to date. Due to the high homology within the K_{ir} family, the channels share a common design of a pore region flanked by two transmembrane domains, identification of site(s) critical for isoform specificity would be an important basis for future development of more specific and potent K_{ir} inhibitors. Using chimeric channels between $K_{ir}2.1$ and $K_{ir}1.1$ and site-directed mutagenesis, we have identified D172 and I176 within M2 segment of $K_{ir}2.1$ as molecular determinants critical for the potency of ML133 mediated inhibition. Double mutation of the corresponding residues of $K_{ir}1.1$ to those of $K_{ir}2.1$ (N171D and C175I) transplants ML133 inhibition to $K_{ir}1.1$. Together, the combination of a potent, $K_{ir}2$ family selective inhibitor and identification of molecular determinants for the specificity provides both a tool and a model system to enable further mechanistic studies of modulation of $K_{ir}2$ inward rectifier potassium channels.

[*]Corresponding authors: Min Li, Department of Neuroscience, Johns Hopkins University School of Medicine, BRB311, 733 North Broadway, Baltimore, MD 21205. minli@jhmi.edu; Craig W. Lindsley, Department of Pharmacology, Vanderbilt University Medical Center, Nashville, TN 37232. craig.lindsley@vanderbilt.edu; tel: 615-322-8700; fax: 615-345-6532.
[†]H.R.W. and M.W. contributed equally to this work

Keywords

Kir2.1; inward rectifying potassium channel; ion channel; mutagenesis; structure-activity-relationship; medicinal chemistry; ion works; patch clamp; high throughput screening; MLPCN

INTRODUCTION

Potassium (K^+) channels are well recognized as targets for treatment of cardiovascular, neurological, renal and metabolic disorders [1–5]. The inward rectifier potassium (K_{ir} or IRK) channels, a subset of potassium selective ion channels, have garnered a great deal of interest as potential therapeutic targets for multiple cardiovascular disorders as well as pain [6–10]. Inwardly rectifying K_{ir} channels allow positively charged K^+ ions to more readily flow in the inward, rather than outward direction, and serve to regulate the resting membrane potential of cells. Structurally, K_{ir} channels are tetramers composed of four membrane-spanning α-helical subunits that surround a water-filled pore through which K^+ ions selectively permeate (Figure 1). Each channel subunit is comprised of two α-helical membrane-spanning domains (M1 and M2) that are separated by an extracellular loop and a region that forms the K^+-selectivity filter. K_{ir} channels also possess a helix bundle crossing motif at the membrane-cytoplasm interface and a large cytoplasmic domain. Seven subfamilies of K_{ir} channels are known ($K_{ir}1$–$K_{ir}7$) and most subfamilies have multiple members (Figure 1) with high sequence conservation in the pore forming domains [6–10]. K_{ir} channels are expressed in variety of tissues with distinct, but overlapping patterns. For example, both $K_{ir}2.1$ and $K_{ir}4.1$ are expressed in astrocytes and glial cells, where $K_{ir}4.1$ is associated with epilepsy in both causative and protective roles [11,12], but the role of $K_{ir}2.1$ in astrocytes and glial cells is not yet clear. $K_{ir}1.1$, $K_{ir}2.3$, $K_{ir}4.1$ and $K_{ir}7.1$ coexist and regulate K^+ ion handling in the kidney tubules [6]. Pharmacological modulation with isoform specificity, or preference, would be of considerable utility in determining the functional roles of these channels, particularly in tissues where multiple isoforms or subtypes may be present. With the recent exception of MLPCN probes for $K_{ir}1.1$ (ROMK) [13,14], small molecule tools to study K_{ir} function are limited to nonselective neurologic and cardiovascular drugs (Figure 2) that happen to possess weak activity toward the K_{ir} channels [10, 15–21]; therefore, the pharmacology of specific channels and their druggability remain in question. However, in 2010, a patent application from Merck described a novel series of $K_{ir}1.1$ inhibitors, represented by **10**, with potent $K_{ir}1.1$ inhibition (IC_{50}s <100 nM), but no selectivity data was reported [22].

The Johns Hopkins Ion Channel Center and the Vanderbilt Specialized Chemistry Center were established as members of the Molecular Libraries Production Center Network (MLPCN) initiated and supported by the NIH Molecular Libraries Roadmap [23]. The MLPCN is a nationwide consortium of facilities that provide high-throughput small molecule screening and medicinal chemistry expertise for the development of chemical probes for use as tools to explore biological targets/pathways for which small molecule tools are unavailable. One such target which lacks the appropriate small molecule tools are the K_{ir} channels, the $K_{ir}2.x$ subfamily and $K_{ir}2.1$, in particular [10]. The inward rectifying potassium channel $K_{ir}2.1$, also known as IRK1 or KCNJ2, is expressed in the heart, brain, vasculature and other tissues [6]. The $K_{ir}2.1$ channel mediates a small hyperpolarizing K^+ current at negative membrane potentials, which plays a major role to establish resting membrane potential and also contributes to the terminal phase of action potential repolarization in diverse cell types [6]. Gain- or loss- of function mutations in the $K_{ir}2.1$ gene lead to cardiac, developmental and other pathologies, including Andersen-Tawil syndrome [24], short QT syndrome (SQT3) [25] and long QT syndrome (LQT7) [26]. Recently, viral introduction of $K_{ir}2.1$ channels has been used as a tool to study the effects of

membrane potential on neuronal cell activity, sensory neuron modulation, as well as cardiac arrhythmias [27,28]. Thus, our MLPCN Centers initiated a campaign to identify and develop, utilizing high throughput Tl^+ flux screening methods combined with automated and conventional patch clamp techniques, Kir2.x selective small molecule tools. This effort ultimately afforded ML133, a potent inhibitor of $K_{ir}2.x$ family channels and the most selective $K_{ir}2.x$ ligand reported to date.

RESULTS AND DISCUSSION

High Throughput Screening to Identify $K_{ir}2.1$ Lead Compounds

Development of isoform specific inward rectifier potassium channel modulators would be of considerable utility in determining their physiological roles and providing a rationale for developing novel therapeutics [6–10]. By combining a Tl^+ flux assay, IonWorks assay, and conventional patch clamp experiments, we were able to identify novel $K_{ir}2.1$ and $K_{ir}2.x$ family inhibitors. The MLSMR library containing 305,616 small-molecules was screened at a concentration of 10 μM employing a thalium (Tl^+) flux assay in 384 well format in a HEK293 cell line stably expressing $K_{ir}2.1$ channels (see Materials and Methods). The assay performed well ($Z' = 0.74$) and afforded 2,545 putative $K_{ir}2.1$ inhibitors, which decreased the Tl^+ responses by more than 3 standard deviation (SD) values from the average of the DMSO control values. Confirmation screening in duplicate then provided 927 active compounds, which were further triaged by counter-screening against the parental HEK293 cell line eliminating another 426 compounds. The remaining 320 confirmed hits with were further counter-screened against hERG and KCNQ9 using Tl^+ flux assays. Based on the chemical structures of the remaining hits, the $K_{ir}2.1$ potency and K^+ ion channel selectivity, a single small molecule remained: CID17367817 (**11**), *N*-(4-methoxybenzyl)-1-(naphthalene-1-yl)methanamine (Figure 3A). Importantly, the PubChem database [29] indicated that **11** had been assayed in 218 MLPCN HTS campaigns, and was active in only two assays not based on $K_{ir}2.1$; thus, **11** had a relatively clean ancillary pharmacology and represented an attractive lead.

Evaluation of Kir2.1 block in electrophysiological experiments

Blocking effects of **11** on Kir2.1 channels were examined in whole cell patch clamp recordings. As shown in Figure 3B, the voltage protocol consisted of a step to − 100 mV to record $K_{ir}2.1$ currents, and then a ramp from −100 mV to 100 mV to monitor the quality of the recording. The protocol was repeated every 10 seconds to determine changes of $K_{ir}2.1$ currents after compound application. Representative traces of the $K_{ir}2.1$ currents before and after 20 minute incubation with 3 μM **11** at pH 7.4 are also shown in Figure 3B. CID17367817 has two hydrophobic benzylic moieties bridged by a linker containing a basic 2° nitrogen, thus, **11** exists in protonated (charged) or non-protonated (neutral) forms, depending on the pH. We therefore examined the effects of pH on inhibition by **11** (predicted pK_a=8.79, from SciFinder) (Figure 3C & D). Increases in bath solution pH enhanced the potency of **11** in inhibiting $K_{ir}2.1$. As shown in Figure 3D, the IC_{50} of **11** was 290 nM at pH 8.5, 1.8 μM at pH 7.4, and 10.0 μM at pH 6.5, respectively. Figure 3C shows representative time courses of **11** inhibition of $K_{ir}2.1$. At pH 8.5, 3 μM of **11** caused complete inhibition of $K_{ir}2.1$ within 5 minutes, while the wash out of compound effects took approximately 10 minutes; at pH 7.4, block by 3 μM required approximately 20 minutes to reach the steady state, and wash out of **11** effects took only 5 minutes; at pH 6.5, 3 μM of **11** had no significant effect on $K_{ir}2.1$ currents over the 20 minute incubation period. Importantly, $K_{ir}2.1$ channel activity itself was not affected by extracellular buffer of pH 6.5 or pH 8.5 (not shown).

Electrophysiological experiments in which block of $K_{ir}2.1$ by **11** was modified by permeant ions along with mapping studies (see below) suggest an intracellular site of action. In support of an intracellular site of action, **11** inhibited $K_{ir}2.1$ channels when directly applied from intracellular side in inside-out patch experiments: at pH 7.4, the IC_{50} for **11** inhibition of $K_{ir}2.1$ was 4.3 μM, close to the IC_{50} (1.9 μM) obtained in whole cell patch clamp recordings, in which **11** is added to the external side at the same pH. Additional inside-out patch clamp experiments suggest that the protonated form of **11** may inhibit $K_{ir}2.1$ channels. At pH 6.5, approximately 99% of **11** molecules would likely be protonated and **11** inhibited Kir2.1 currents more effectively than at pH 7.4 or pH 8.5, at which fewer molecules of **11** are protonated (pH 6.5, IC_{50}=2.6 μM; pH 7.4, IC_{50}=4.3 μM; pH 8.5, IC_{50}=12.5 μM). The pH-dependence of block by internally applied **11** was less pronounced, and was the inverse of the pH-dependence of extracellularly applied **11** as discussed above. These results suggest a mechanism in which extracellular pH regulates inhibition of $K_{ir}2.1$ by **11**, possibly by changing the ratio of protonated and non-protonated forms of **11** and causing differential membrane permeation.

Small molecules that are more water-soluble when ionized and more lipid soluble when un-ionized. **11** would likely permeate cell membranes in the neutral form, which would be more prevalent at high pH values. As such, **11** would likely enter cells more readily in the de-protonated form and would then be re-protonated at the intracellular side (pH 7.4 maintained by HEPES in pipette solution) leading to intracellular accumulation. Some simple calculations support this explanation. At steady state, the concentrations of the non-protonated form of **11** should be equivalent inside and outside of the cell. The relative concentrations of protonated and unprotonated forms of **10** can be calculated based on the predicted pKa (8.79) of **11**. At pH 6.5 on the external side, the ratio of total concentration of extracellular **11** versus intracellular **11** is (195+1):(24.5+1)=1:0.13. At pH 7.4, the intracellular and extracellular pH values are identical as will be total concentrations of **11**. At external pH 8.5, the ratio of total concentration of extracellular **11** versus intracellular **11** is (1.9+1):(24.5+1)=1:9.09. This yields an expected 70-fold increase in intracellular concentration of **11** when extracellular pH is elevated from 6.5 to 8.5, which approximates the observed 34-fold change in IC_{50} for channel block. These estimates of external pH effects on intracellular concentration of **11** can be used to calculate expected IC_{50} values for channel block at different external pH values, assuming that extracellular pH changes do not directly change channel sensitivity to block by **11**. Using the observed IC_{50} of 1.8 μM at external pH 7.4 as a reference point, at external pH 6.5, the predicted IC_{50} value of 14.6 μM agrees with the observed value (10.0 μM), and at external pH 8.5, the predicted IC_{50} value of 0.21 μM again agrees with the observed value (0.29 μM).

To further validate our model, we set out to test compound **14k** (Figure 5), a derivative with a different pKa due to methylation of the central nitrogen. The measured IC_{50} of **14k** is 31 μM at pH 7.4 and 9.2 μM at pH 8.5, a 3.37 fold decrease of IC_{50} at pH 8.5 compared with pH 7.4. The predicted pKa of compound **14k** is 7.93. Using calculations as described above, the expected intracellular **14k** will increase 3.45-fold at pH 8.5 compared with pH 7.4, which can account for the 3.37-fold decrease of IC_{50} over this pH range. Thus, this model is consistent with the observed pH-dependent changes in IC_{50} values for block and the kinetics of inhibition, but other models may also be consistent with the present data. Thus, focus now shifted towards developing structure activity relationships (SAR) for **11**.

Chemical Lead Optimization

For the chemical lead optimization of CID17367817 (**11**), we divided the lead compound into three sections denoted western aryl, linker and eastern aryl (Figure 4A). First generation libraries held either the naphthyl moiety or the 4-methoxybenzyl moiety constant and surveyed alternative aryl moieties (2 × 20 members). The chemistry for these first

generation libraries was straightforward [30] and involved a reductive amination sequence with an aryl aldehyde **12** and a benzyl amine **13** with $NaB(OAc)_3H$ and conversion of the analogs **14** to the HCl salt prior to screening in manual patch clamp at pH 8.5 (Figure 4B). In addition, the original hit was re-synthesized as the HCl salt, and assigned CID781301 (Pubchem SID85281105/SID 87457855). As shown in Figure 5, the re-synthesized **11** confirmed with a $K_{ir}2.1$ IC_{50} of 290 nM in manual patch clamp experiments. Clear SAR was established, and we quickly discovered that the 4-methoxybenzyl moiety was critical for $K_{ir}2.1$ activity. Libraries holding the naphthyl moiety constant and surveying alternate aryl groups for the 4-methoxybenzyl group lost all activity. However, modest $K_{ir}2.1$ activity ($K_{ir}2.1$ IC_{50} <5 μM) could be retained when the 4-methoxybenzyl group was maintained as in **14a-k**. The 4-chloro and 3-chlorobenzyl analogs (**14a**, CID 44483168; **14b**, CID 44483172) were equipotent ($K_{ir}2.1$ IC_{50} = 0.77 μM and 1.06 μM, respectively). The 4-*tert*-butylbenzyl analog (**14d**, CID 44483167) was comparable to **14b** ($K_{ir}2.1$ IC_{50} = 1.39 μM). Substitution in the 2-position, in the form of either a 2-methylbenzyl (**14e**, CID 44483176), 2,4-dichlorobenzyl (**13c**, CID 44483171), or 2-chlorobenzyl (**14j**, CID 44483175) analogs led to diminished potency, 5.15 μM, 3.89 μM, and 13.88 μM respectively. All other analogs led to either inactive compounds, or much reduced potency compared to re-synthesized **11** (CID 781301). Figure 5B provides an overview of the observed SAR. In addition to evaluating the western and eastern aryl groups, we also explored alternative linker moieties. Replacement of the NH with an oxygen led to a complete loss of $K_{ir}2.1$ activity as did replacement of either benzylic CH_2 with a carbonyl to provide the analogous amide congeners. Introduction of alkyl groups at the benzylic positions also led to a significant diminution in $K_{ir}2.1$ potency. Thus, the re-synthesized HTS hit **11** proved to be the the most potent $K_{ir}2.1$ inhibitor reported in this study, a rare instance where the HTS lead could not be improved upon. At this point, **11** was declared an MLPCN probe and assigned the probe identifier ML133.

Selectivity of ML133 inhibition of K_{ir} family channels

To test whether ML133 exhibits selectivity over other inward rectifiers, we measured its effects on other $K_{ir}2.x$ channels, including $K_{ir}2.2$ [41], $K_{ir}2.3$ and $K_{ir}2.6$, and all showed similar IC_{50} values for ML133 block compared with $K_{ir}2.1$ (Table 1). In contrast, $K_{ir}4.1$ and $K_{ir}7.1$ were much less sensitive displaying higher IC_{50} values, 76 μM and 33 μM respectively for ML133 block. Notably, $K_{ir}1.1$, also known as ROMK, is essentially insensitive to ML133 (Table 1). $K_{ir}2.1$ and $K_{ir}1.1$ are two highly conserved channel proteins with 54% similarity over the entire amino acid sequence and 67.7% within the transmembrane and pore domains (M1-P-M2) [10]. In addition to the relatively clean profile in over 218 MLPCN assays, ML133 was evaluated in Ricerca's Lead Profiling Screen [32], which employs 68 radioligand binding assays across numerous GPCRs, ion channels and transporters. Overall, ML133 displayed clean ancillary pharmacology and was inactive at both L- and N-type calcium channels as well as several other potassium channels including hERG. Thus, ML133 is the most potent and selective $K_{ir}2.x$ family selective small molecule reported to date.

ML133 was also evaluated in our tier 1 *in vitro* DMPK battery to further establish its utility as a small molecule probe. In CYP_{450} assays, ML133 was clean against 3A4 and 2C9 (IC_{50} >30 μM), displayed moderate inhibition of 1A2 (IC_{50} = 3.3 μM) but proved to be a potent inhibitor of 2D6 (IC_{50} = 0.13 μM). In addition, ML133 was highly protein bound (>99%) in both human and rat and also displayed high intrinsic clearance in both species. Thus, the utility of ML133 is limited to *in vitro* studies of the $K_{ir}2.x$ family.

Possible pore blocking mechanism for ML133

Ion channel pore blockers may display a phenomenon termed “knock-off”, where, in some cases, an intracellular pore blocker can be displaced from its binding site by inward K^+ ion flux [13,14]. Typically, such an effect is more readily observed with a weaker blocker [21]. The interaction between M133 and wild-type $K_{ir}2.1$ may be too strong to be significantly influenced by these mechanisms in the current experimental settings (Figure 6). In order to further explore the mechanism of inhibition of this class of K_{ir} channel blockers, we took advantage of a *bis*-4-methoxybenzylamine analog of ML133, **14g** (CID 44483166), with an IC_{50} for $K_{ir}2.1$ block of 35 μM at pH 7.4. At 30 μM, **14g** showed a dramatic “knock-off” profile in the wild-type $K_{ir}2.1$ channel (pH 7.4, 140 mM $K_{outside}$). The apparent knock-off of **14g** by K^+ ions diminished when the extracellular K^+ was reduced to 4 mM (Figure 6D) in agreement with a mechanism in which blockers bind to a site in the permeation pathway and interact with permeant ions. In this experiment (Figure 6D), the membrane potential was stepped from −80 mV to −180 mV to maintain a similar absolute change in membrane potential and a similar driving force for K^+ ions relative to the potassium reversal potential, although the channel conductance is decreased relative to 140 mM potassium bath solution. These data argue against a direct effect of membrane potential causing the time-dependent changes in channel block.

Chimeric channels reveal critical domain(s) in $K_{ir}2.1$ mediating ML133 inhibition

To carefully examine the effect of ML133 on $K_{ir}1.1$, we tested ML133 up to 300 μM after a prolonged incubation of more than 10 minutes (Figure 7A). The currents with or without drug essentially overlapped. The leak current was negligible since barium inhibited over 85% of the $K_{ir}1.1$ current at the end of the recording. At pH 8.5, ML133 did show enhanced potency for $K_{ir}1.1$ block, with estimated IC_{50} of 85.5 μM (Figure 7B).

In order to identify the molecular region(s) conferring high affinity inhibition of $K_{ir}2.1$, we evaluated a series of chimeric channels between $K_{ir}2.1$ and $K_{ir}1.1$ as shown in Figure 7C [33]. These chimeric channels are fully functional and display gating properties similar to that of $K_{ir}2.1$ or $K_{ir}1.1$ depending on their amino acid attribution. At a test concentration of 30 μM of ML133 (pH 7.4), both chimeras C8 and C108 were strongly inhibited (>90%), similar to wild-type $K_{ir}2.1$. However, chimeras C25 and C13 remained resistant to 30 μM ML133, comparable to that of wild-type $K_{ir}1.1$. These results suggest that M1 and/or M2 transmembrane domains contain the critical molecular determinant(s) for ML133 inhibition of $K_{ir}2.1$.

Identification of critical residues for ML133 inhibition of Kir2.1

There are two potential interpretations one may draw from results of chimeric studies. First, the M1 and/or M2 segments in $K_{ir}2.1$ contain key residues that confer the binding to ML133 and subsequent sensitivity to inhibition. Alternatively, The M1 and/or M2 regions of $K_{ir}1.1$, in fact, can interact with the compound, but have certain “toxic” residues/effects that prevent ML133 from causing inhibition. To address this, we first compared the amino acid sequences among all tested K_{ir} channels (Table 1). Recent advances in understanding of potassium channel structure, based on the 3.2 Å crystal structure of $K_{ir}2.2$, suggest that the M2 transmembrane domain forms the inner lining of the $K_{ir}2.x$ ion conducting pathway [33]. Intriguingly, within M2 region there are several residues that appear to be conserved in correlation with the ML133 sensitivity. Considering that the inhibitory site appears to be accessible from the intracellular side, we began to focus our mutagenesis on those residues proximal to the cytoplasmic face of the pore domain. Sequence comparison analysis is consistent with a critical role for several residues, particularly in positions corresponding to D172/I176 in Kir2.1 channels (Table 1).

In order to evaluate their relevance, we converted these residues to $K_{ir}1.1$ residues in otherwise wild-type $K_{ir}2.1$ background (Figure 8). The Kir2.1 D172N single mutation greatly reduced the potency of ML133 inhibition, increasing the IC_{50} to 15 μM, while $K_{ir}2.1$ D172N/I176C double mutation further reduced ML133 potency with an IC_{50} of 45 μM. Conversely, if these residues are key mediators for the ML133 sensitivity, one would expect the changes of $K_{ir}1.1$ residues to those of $K_{ir}2.1$ would confer sensitivity to ML133. The C25 chimera has the transmembrane M1-Pore-M2 domain of $K_{ir}1.1$ but $K_{ir}2.1$ cytoplasmic domain, hence being used for these experiments. As shown in Figure 8C, with merely about 30% inhibition by 100 μM ML133, wild-type C25 chimera exhibited little sensitivity toward ML133 at pH 7.4. The C25 N172D single mutant shifted the IC_{50} to 75 μM, suggesting $K_{ir}2.1$ D172 may be involved in ML133 inhibition. The C25 N172D/M175I/C176I triple mutant almost completely restored sensitivity to ML133 inhibition, with IC_{50} value of 5.8 μM, which is comparable to the IC_{50} of 1.9 μM for $K_{ir}2.1$. Since $K_{ir}2.1$ I175 varies among $K_{ir}2.x$ family ($K_{ir}2.2$, $K_{ir}2.3$ and $K_{ir}2.6$ have the same methionine residual as $K_{ir}1.1$ and are sensitive to ML133), $K_{ir}2.1$ I176 rather than Kir2.1 I175 may serve as a more important determinant of ML133 binding. We therefore constructed N171D single or N171D/C175I double mutants in $K_{ir}1.1$ background in attempt to engineer the ML133 sensitivity (Figure 8D). Indeed, IC_{50} of $K_{ir}1.1$ N171D was 83.6 μM and IC_{50} of $K_{ir}1.1$ N171D/C175I double mutant was 64.0 μM, both of which are significantly sensitized compared to wild-type $K_{ir}1.1$. Therefore, these data suggests that $K_{ir}2.1$ D172 and I176 are necessary for ML133 inhibition, and can partially transfer ML133 sensitivity to insensitive $K_{ir}1.1$ channels.

The side-chain groups corresponding to $K_{ir}2.1$ D172 and I176 in $K_{ir}2.1$ are positioned to face the central region of the pore in the crystal structure of $K_{ir}2.2$ (Figure 9A). The distance from $K_{ir}2.1$ D172 to I176 of the same subunit is estimated to be 6.24 Å based on the crystal structure of $K_{ir}2.2$ channel [33]. In comparison, the distance between the central protonable nitrogen to one of the aromatic rings is approximately 5.08 Å, sufficient for M133 to bridge $K_{ir}2.1$ D172 and I176 as shown in a homology model of $K_{ir}2.1$ constructed [34,35] from the $K_{ir}2.2$ crystal structure (Figure 9B). Based on the $K_{ir}2.2$ crystal structure [33], $K_{ir}2.1$ I176 likely forms hydrophobic seals beneath the central cavity to close off the pore section leading to the cytoplasm. This signature structure is unique for some eukaryotic ML133 sensitive K_{ir} channels such as $K_{ir}2.1$ (I176) and $K_{ir}6.2$ (L164). In contrast, K_{ir} channels lacking this motif ($K_{ir}1.1$, $K_{ir}3$, $K_{ir}4.1$, and $K_{ir}7.1$) displayed weaker block by ML133.

Structurally, the hydrophobic girdle at $K_{ir}2.1$ I176 is narrow enough to prevent the passage of water and hydrated K^+ ions, suggesting a role in gating for $K_{ir}2.1$ I176. Functionally, $K_{ir}2.1$ I176C is readily inhibited by MTSET using substituted-cysteine accessibility method (SCAM). The SCAM inhibition kinetics at his site are the fastest among all pore lining residues [36], and far faster than for non-pore lining residues [37]. These results agree with structural data and indicate that $K_{ir}2.1$ I176 is accessible from cytoplasma side, and possibly having a role in Kir channel gating. Indeed, $K_{ir}2.1$ I176 analogous mutation in $K_{ir}3.2$ V188G (A) is constitutively active in the absence of active G protein subunits, suggesting the participation of $K_{ir}3.2$ V188 in channel gating [38]. Analogous mutation in $K_{ir}6.2$ (L164P) is also constitutively active and causes permanent neonatal diabetes mellitus (PNDM). The mutant channel can no longer be inhibited by intracellular ATP and displays altered SUR1 modulation [39]. These data support a role for $K_{ir}2.1$ I176 and analogous residues in K_{ir} channel gating.

ML133 can be used as a probe not only for $K_{ir}2.1$ but also for $K_{ir}2.x$ family. It may be particular useful to parse out the physiological role of $K_{ir}2.x$ current in distal tubulule of kidney, where $K_{ir}2.3$ are expressed at the basolateral side of the cell and Kir1.1 are expressed in the apical side of the cell. It has been speculated that the role of $K_{ir}2.3$ is to

recycle K^+ back into the cell in order to maintain the function of Na^+/K^+ pump, but this hypothesis has never been tested due to lack of probe differentiating $K_{ir}2.3$ from $K_{ir}1.1$.

Besides abundant expression in pancreatic cells, $K_{ir}6.2$ channel is only moderately expressed in the heart, skeletal muscle, and brain, together with different SUR subunits, the complex is also known as K_{ATP} channel. $K_{ir}2.x$ expression is usually much higher in these tissues[6]. In addition, K_{ATP} channel is highly inhibited by endogenous ATP and is not constitutively active as $K_{ir}2.x$ does, thus even when K_{ATP} channel co-expressed with $K_{ir}2.x$, they will probably remain silent and not contribute to the K^+ conductance. Under certain circumstances when K_{ATP} channel activity become prominent, like in smooth muscle[6], one can use specific K_{ATP} channel inhibitors like glibenclamide (IC_{50}=3 nM) to abolish K_{ATP} channel current before using ML133 to study $K_{ir}2.x$ function.

CONCLUSION

An HTS of more than 300,000 small molecules within the MLPCN was performed to identify modulators of $K_{ir}2.1$ function employing Tl^+ flux assay. Here we report one potent $K_{ir}2.1$ inhibitor, ML133, which inhibits $K_{ir}2.1$ with IC_{50} of 290 nM at pH 8.5 and 1.8 μM at pH 7.4, but exhibits little selectivity against other member of Kir2.x family channels. However, ML133 has no effect on $K_{ir}1.1$ (IC_{50} > 300 μM), and displays weak activity for $K_{ir}4.1$ (76 μM) and $K_{ir}7.1$ (33 μM). In addition, ML133 was inactive in all but two of 213 MLPCN HTS assays not directed to K_{ir} channels as well as displaying a clean profile in a radioligand binding panel of 68 GPCRs, ion channels and transporters. Therefore, ML133 is the most selective small molecule inhibitor of the $K_{ir}2.x$ family reported to date. Moreover, a multidimensional library effort failed to improve upon the potency of the HTS hit – a rare case in our experience. Detailed characterization, employing chimeras, mutagenesis and knock-off experiments, suggests a mechanism for inhibition of $K_{ir}2.x$ channels in which ML133 binds to a site in the ion conducting pore formed by M2 transmembrane domains. These lines of evidence are consistent with a pore blocking mechanism for ML133 and suggest a putative interaction site. Based on the crystal structure of $K_{ir}2.2$, we constructed a $K_{ir}2.1$ homology model, and developed a manual docked hypothesis for energy minimized ML13 that is based on the mutagenesis studies. In addition, comparison of the $K_{ir}2.1$ model with a model for $K_{ir}1.1$ illustrate a more open conformation in the floor of the putative ML133 binding site. Further optimization efforts may employ these new models to guide ligand refinement.

MATERIALS/METHODS

Cell line, transfection reagent and chemicals

For conventional patch clamp experiments, the $K_{ir}2.1$ stable cell line and HEK 293 cell were cultured in DMEM/F12 medium, supplemented with 10% Fetal Bovine Serum (FBS), 50 IU/mL penicillin, 50 ug/mL streptomycin. Transient transfection on HEK293 cell was performed 48 hour before experiment using Lipofectamine LTX kit (Invitrogen, Carlsbad, CA). Usually, a total of 1 μg of DNA/3 μl Lipofectamine was used for transfection in one 35 mm dish. Compound ML133 was originally from Molecular Library Small Molecule Repository (MLSMR) and synthesized as a dry powder by the Vanderbilt Specialized Chemistry Center. Other compounds for SAR analysis were also provided by the Vanderbilt Specialized Chemistry Center.

Molecular Biology

Mouse $K_{ir}2.1$ pcDNA3 is as previously described [17]. Rat $K_{ir}1.1$ pEGFP-N3, human $K_{ir}2.6$ pcDNA3, rat $K_{ir}4.1$ in pCruz-myc vector and Human $K_{ir}7.1$ in pcDNA3 vector were gifts

from Dr. Chou-Long Huang (University of Texas Southwestern Medical Center at Dallas). Chimeras between $mK_{ir}2.1$ and $rK_{ir}1.1$, namely C108, C8, C13, C25, were kindly made by Dr. Henry Sackin (Rosalind Franklin University of Medicine and Science, North Chicago, IL) [31]. The chimeras were originally in pSPORT vector. The inserts were then amplified by PCR and subcloned into pIRES2-EGFP vector by XhoI and PstI sites. Human $K_{ir}2.2$ (pCXN2 vector) and human $K_{ir}2.3$ (pcDNA3 vector) were gift from Dr. Anthony Collins (University of Belfast, Northern Ireland, UK). Rat $K_{ir}6.2$ was cloned into pcDNA1 vector. Hamster-SUR1 was cloned into pECE vector and co-transfected with $K_{ir}6.2$ during experiments. Point mutations were generated by site-directed mutagenesis (QuikChange kit; Stratagene) and confirmed by sequencing.

Conventional patch clamp

The electrodes were pulled from borosilicate glass capillaries (World Precision Instruments, Sarasota, FL). Pipette resistance was around 3–4 MΩ. Whole-cell currents of $K_{ir}2.1$ were recorded using an Axopatch 200B amplifier. The bath and pipette solutions contained 140 mM KCl, 2 mM $MgCl_2$, 2 mM $CaCl_2$, 10 mM HEPES (pH 7.4) and 140 mM KCl, 2 mM EDTA, 10 mM HEPES (pH 7.4), respectively. To apply the compound, 7–10 mL of compound solution was introduced by a 10 mL syringe into recording chamber containing 0.5 mL bath solution. Excessive solution was removed by suction. To record currents, voltage was stepped from 0 mV holding potential to −100 mV (500 ms) with an interval of 30 seconds. Capacitance compensation and 75% series resistance compensation were applied. Currents were filtered at 1 kHz, and data were acquired at 5 kHz with a Digidata 1322A computer interface and pClamp 9.2 software (Molecular Devices Corp.). To check the quality of seal during recording, each voltage step was followed by a ramp protocol (500 ms, from −100 mV to 100 mV). Cells losing seal during recording were identified by a sudden increase of outward current in the ramp protocol, and were not used.

Thallium-based fluorescence assay

Activity of potassium channels was monitored by the influx of thallium (Tl^+), a surrogate ion for potassium. Thallium influx was detected through the use of a thallium-sensitive fluorescent dye, FluxOR (Invitrogen, Carlsbad, CA, Cat #F10017). Cells were seeded at 15,000 cells per well into BD Biocoat poly-D-Lysine coated 384-well-plates (BD, Cat# (35)6663 and Lot #8163495) using a Multidrop (Thermo scientific, Hudson, New Hampshire) and incubated overnight at 37 °C and 5% CO_2. The thallium-based fluorescence assay for $K_{ir}2.1$ was performed according to the manufacture's recommended protocol. Briefly, medium was removed; cells were incubated with 1x FluxOR solution, 25 μL/well, for 90 minutes at room temperature (RT) in the dark; the 1x FluxOR solution was replaced by assay buffer (Hanks Balanced Salt Solution containing 5.8 mM potassium; product # 14065, Gibco, NY), 20 μL/well; test compounds in 7.5x stock of final concentration (10 μM) from a 10 mM stock supplied by the NIH Molecular Libraries Small Molecule Repository (BioFocus DPI, San Francisco, CA) or controls in assay buffer were then added to cells, 4 μL/well; 20 minutes later, cell plates were loaded to Hamamatsu FDSS 6000 kinetic imaging plate reader; after establishing fluorescence baseline by 1 Hz scanning for 10 seconds, Tl^+ influx was triggered by addition of 6 μL/well of 5x stimulus buffer (containing 25 mM K_2SO_4 and 7 mM Tl_2SO_4) and fluorescence measurement was continued at 1 Hz for another 110 seconds. Controls wells contained assay buffer (IC_0), or IC_{100} of chlorpromazine (all with DMSO concentrations matched to that of test compounds). The fluorescence ratio readouts were calculated by F(max−min)/F0, as well as Z prime factors from the average and standard deviation for negative and positive controls in each plate. Hit selection was based on the B scores [40] for test compounds calculated from the fluorescence ratios. If the B score of the test compound was less than minus 3 times the standard deviation (SD) of the B scores of ratios of the library compounds (<=-3*SD), and

the B score of initial fluorescence intensity is within 2 times the standard deviation of the B scores of the library compounds, the compound is designated as an inhibitor/blocker of $K_{ir}2.1$ channels. Otherwise, it is designated as inactive.

Automated patch clamp

Automated patch-clamp experiments were performed using population patch clamp mode of automated voltage clamp recording with an IonWorks Quattro (Molecular Devices, Sunnyvale, CA). Briefly, compound effects on the $K_{ir}2.1$ channel were tested at 25 μM. The HEK-293 cells stably expressing $K_{ir}2.1$ channels were dislodged using 0.25 % Trypsin/EDTA and re-suspended at 2×10^6 cells/mL in external buffer (140 mM K-gluconate, 1.8 mM $CaCl_2$, 1 mM $MgCl_2$, 10 mM HEPES, 10 mM Glucose, pH 7.4 or otherwise specified). Cells were then dispensed to the 384-well population patch clamp (PPC) plate. After dispensing, seal resistance of cells was measured for each well and cells were perforated on the internal solution side by incubation with 0.1 mg/mL amphotericin B in internal buffer (40 mM KCl, 100 mM K-gluconate, 1 mM $MgCl_2$, 5 mM HEPES, 2 mM $CaCl_2$ pH 7.2). Activity of $K_{ir}2.1$ was then measured with the following recording protocol: hold cells at +10 mV, step to −100 mV for 800 ms, back to +10 mV for 600 ms and run a ramp from −100 mV to +100 mV in 800 ms followed by a step back to +10 mV. Aliquots of 3.5 μl 3X compounds (final concentration 25 μM) prepared using external buffer, as well as controls with DMSO concentrations matched to that of test compounds, were dispensed to individual wells in the patch plate and incubated for 4 minutes. Currents were measured after compounds addition with the same protocol. Percentage of inhibition was calculated as (Ipre −Ipost)/Ipre*100% for each compound. Compared to negative controls, if a compound caused 3SD or more decrease in current amplitude, it was classified as an inhibitor.

Statistics

Manual electrophysiology data were analyzed using pClamp 9.2 followed by Origin 6 (OriginLab Corporation, Northampton, MA). The fluorescence data of the thallium-based flux assay were analyzed by manufacturer's software package provided by Hamamatsu Photonics (Hamamatsu, Japan). Automated patch clamp data were analyzed in IonWorks 2.0.4.4 (Moledular Devices Corp., Sunnyvale, CA) and then exported for further analysis by Excel (Microsoft, CA) and Origin 6.

Structure-based Visualization and Putative ML133 Binding Site Models

Molecular models for the putative ML133 binding site for $K_{ir}2.1$ and $K_{ir}1.1$ tetramers were generated using the template structure of chicken $K_{ir}2.2$ (PDB_ID: 3JYC) and the sequence alignment of Tao, et al. [32]. Briefly, the backbone coordinates of the putative binding site region of the tetrameric $K_{ir}2.2$ structure were copied and side chains replaced for human $K_{ir}2.1$ and $K_{ir}1.1$ according to the alignment of Tao, et al. using the most probable amino acid rotamers for each residue from a backbone dependent rotamer library [37] as implemented in UCSF Chimera [38]. Low energy conformers for the ML133 probe molecule were generated using a stochastic search (10,000 cycles) of all rotatable bonds as implemented in MOE (Chemical Computing Group; Montreal, Canada). The lowest energy structure returned from this search was subjected to 500 steps of gradient energy minimization using the Merck force field (MMFF94) partial charges and then manually docked into a putative binding site (containing the identified mutations) just below the pore region of the $K_{ir}2.1$ model. The manually docked model was utilized only for visualization and comparison with the $K_{ir}1.1$ model to facilitate hypothesis generation for evaluation of potential intermolecular structure activity relationships. Molecular graphics were generated and rendered using the UCSF Chimera package from the Resource for Biocomputing, Visualization, and Informatics at the University of California, San Francisco (supported by NIH P41 RR001081).

Compound Synthesis and Characterization

General Experimental—All reagents were purchased from Sigma-Aldrich Corp., TCI America, and Rieke Metals, Inc. and were used without purification. All polymer supported reagents were purchased from Biotage, Inc. Analytical thin-layer chromatography (TLC) was performed on 250 μm silica gel plates from Sorbent Technologies. Visualization was accomplished via UV light, and/or the use of ninhydrin and potassium permanganate solutions followed by application of heat. Chromatography was performed using Silica Gel 60 (230–400 mesh) from Sorbent Technologies or Silica RediSep R_f flash columns on a CombiFlash R_f automated flash chromatography system. All ^1H and ^{13}C NMR spectra were recorded on a Bruker AV-400 (400 MHz) instrument. Chemical shifts are reported in ppm relative to residual solvent peaks as an internal standard set to δ 7.26 and δ 77.16 ($CDCl_3$). Data are reported as follows: chemical shift, multiplicity (s = singlet, d = doublet, t =triplet, q = quartet, br = broad, dd=doublet of doublets, dq=doublet of quartets, td =triplet of doublets, pd = pentet of doublets, m = multiplet), coupling constant (Hz), integration. Low resolution mass spectra (LCMS) were obtained on an Agilent 1200 LCMS with electrospray ionization. High resolution mass spectra (HRMS) were recorded on a Waters Qtof-API-US plus Acquity system with ES as the ion source. Analytical high pressure liquid chromatography (HPLC) was performed on an Agilent 1200 analytical LCMS with UV detection at 214 nm and 254 nm along with ELSD detection.

General Library Synthesis of 14a–k—To a 4 mL vial was placed 0.5 mmol of amine, 0.5 mmol of aldehyde and diluted with 2 mL of DCE. MP-$NaB(OAc)_3H$ (3 equiv. 1.5 mmol) was added and the vial placed on a rotator overnight. Vials were then filtered to remove the resin, concentrated and purified by mass-0directed preparative HLPC to analytical purity (>98% by 214 nm, 254 nm and ELSD).

ML133 (11). *N*-(4-methoxybenzyl)-1-(naphthalen-1-yl)methanamine (Figure 4B)—To a solution of (4-methoxyphenyl)methanamine (1.15 mL, 8.83 mmol) in DCE (25 mL) was added 1-naphthaldehyde (0.69 mL, 5.08 mmol). After 15 min, $NaB(OAc)_3H$ (2.80 g, 13.23 mmol) was added portion wise over 5 min. After 12 h, water (25 mL) was added to the rxn and after another additional 1h, transferred to DCM:water (1:1; 250 mL). The organic layer was separated, washed with water (2 × 50 mL), and passed through a Phase separator. After concentration, the desired product was purified by preparative HPLC to afford an off-white solid (0.70 g, 50%): Analytical LCMS: single peak (214 nm), 1.123 min; ^1H NMR (400 MHz, *d6*-DMSO): δ 9.25 (br s, 1H), 8.07 (*d*, *J* = 8.0 Hz, 1H), 8.00 (*d*, *J* = 8.0 Hz, 2H), 7.68-7.48 (m, 6H), 7.01 (*d*, *J* = 8.4 Hz, 2H), 4.59 (s, 2H), 4.26 (s, 2H), 3.77 (s, 3H); HRMS, calculated for $C_{19}H_{20}NO$ (M+ H+), 278.1545; found 278.1544. HCl Salt Formation: To a solution of the amine in DCM (0.2 M) at 0 °C was added 4 M HCl in 1,4-dioxane (5 equiv.) dropwise. After 15 min, the ice bath was removed. The solvent was removed after additional 30 min at RT to provide a pure HCl salt of the appropriate amine.

Acknowledgments

We thank members of both the Li laboratory and JHICC for valuable discussions and comments on the manuscript, and Ms Alison Neal for editing the document. Katrina Brewer, Frank Byers, Annie Blobaum and Ryan Morrison are thanked for the *in vitro* DMPK data. This work is supported by grants from the National Institutes of Health (GM078579 and MH084691 to M.L., U01MH087965 to C.L.).

ABBREVIATIONS

K_{ir}	Inward rectifying potassium channel
HTS	High throughput screening

IC_{50}	Half maximal inhibitory concentration
N_H	Hill coefficient
SAR	Structure activity relationship
PNDM	Permanent neonatal diabetes mellitus

References

1. Littleton JT, Ganetzky B. Ion channels and synaptic organization: analysis of The Drosophila genome. Neuron. 2000; 26 (1):35–43. [PubMed: 10798390]
2. Hille, B. Ion channels of excitable membranes. Sunderland, Mass: Sinauer; 2001. Chapter 5: Potassium Channels and Chloride Channels; p. 131-168.
3. Jessell, TM.; Kandel, ER.; Schwartz, JH. Principles of Neural Science. 4. New York: McGraw-Hill; 2000. Chapter 6: Ion Channels; p. 105-124.
4. Lotshaw DP. Biophysical, pharmacological, and functional characteristics of cloned and native mammalian two-pore domain K+ channels. Cell Biochemistry and Biophysics. 2007; 47 (2):209–56. [PubMed: 17652773]
5. Doyle DA, Morais CJ, Pfuetzner RA, Kuo A, Gulbis JM, Cohen SL, Chait BT, MacKinnon R. The structure of the potassium channel: molecular basis of K^+ conduction and selectivity. Science. 1998; 280 (5360):69–77. [PubMed: 9525859]
6. Hibino H, Inanobe A, Furutani K, Murakami IF, Kurachi Y. Inwardly rectifying potassium channels: their structure, function, and physiological roles. Physiol Rev. 2010; 90(1):291–366. [PubMed: 20086079]
7. Kubo Y, Adelman JP, Clapham DE, Jan LY, Karschin A, Kurachi Y, Lazdunski M, Nichols CG, Seino S, Vandenberg CA. International Union of Pharmacology. LIV. Nomenclature and molecular relationships of inwardly rectifying potassium channels. Pharmacol Rev. 2005; 57 (4):509–26. [PubMed: 16382105]
8. Abraham MR, Jahangir A, Alekseev AE, Terzic A. Channelopathies of inwardly rectifying potassium channels. Faseb J. 1999; 13 (14):1901–1910. [PubMed: 10544173]
9. Ehrlich JR. Inward rectifier potassium currents as a target for atrial fibrilation therapy. J Cardiovasc Pharmacol. 2008; 52:129–135. [PubMed: 18670367]
10. Bhave G, Lonergan D, Chauder BA, Denton JS. Small-molecule modulaotrs of inward rectifier K+ channels: recent advances and future possibilities. Future Med Chem. 2010; 2(5):757–774. [PubMed: 20543968]
11. Horio Y. Potassium channels of glial cells: distribution and function. Jpn J Pharmacol. 2001; 87(1): 1–6. [PubMed: 11676192]
12. Seifert G, Schilling K, Steinhauser C. Astrocyte dysfunction in neurological disorders: a molecular perspective. Nat Rev Neurosci. 2006; 7(3):194–206. [PubMed: 16495941]
13. Lewis LM, Bhave G, Chauder BA, Banerjee S, Lornsen KA, Fallen K, Lindsley CW, Weaver CD, Denton JS. High-throughput screening reveals a small-molecule inhibitor of ROMK and Kir7.1. Mol Pharm. 2009; 76:1094–1103.
14. Bhave G, Chauder BA, Liu W, Dawson ES, Kadakia R, Nguyen TT, Lewis LM, Meiler J, Weaver CD, Satlin LM, Lindsley CW, Denton JS. Development of a selective small-molecule inhibitor of Kir1.1, the renal outer meduallary potassium channel'. Mol Pharm. 2011; 79:42–50.
15. Ponce-Balbuena D, Lopez-Izquierdo A, Ferrer T, Rodriguez-Menchaca AA, Arechiga-Figueroa IA, Sanchez-Chapula JA. Tamoxifen inhibits inward rectifier K+ 2.x family of inward rectifier channels by interfering with phosphatidylinositol 4,5-bisphosphate-channel interactions. J Pharmacol Exp Ther. 2009; 331(2):563–573. [PubMed: 19654266]
16. Rodriguez-Menchaca AA, Picollo A, Carbonara G, Fracchiolla G, Tortorella P, Loidice F, Laghezza A, Babini E, Zifarelli G, Pusch M, Camerino DC. The molecular basis of chloroquine block of the inward rectifier Kir2.1 channel. Proc Natl Acad Sci USA. 2008; 105(4):1364–1368. [PubMed: 18216262]

17. Sun H, Liu X, Xiong Q, Shikano S, Li M. Chronic inhibition of cardiac Kir2.1 and HERG potassium channels by celastrol with dual effects on both ion conductivity and protein trafficking. J Biol Chem. 2006; 281(9):5877–5884. [PubMed: 16407206]
18. Zaks-Makhina E, Li H, Grishin A, Salvador-Recatala V, Levitan ES. Specific and slow inhibition of the kir2.1 K+ channel by gambogic acid. J Biol Chem. 2009; 284(23):15432–15438. [PubMed: 19366693]
19. Zaks-Makhina E, Kim Y, Aizenman E, Levitan ES. Novel neuroprotective K+ channel inhibitor identified by high-throughput screening in yeast. Mol Pharmacol. 2004; 65(1):214–219. [PubMed: 14722253]
20. Lopez-Izquierdo A, Ponce-Balbuena D, Ferrer T, Rodriguez-Menchaca AA, Sanchez-Chapula JA. Thiopental inhibits fucntion of different inward rectifying potassium channel isoforms by a simialr mechanism. Eur J Pharmacol. 2010; 638:33–41. [PubMed: 20447386]
21. Shin HG, Lu Z. Mechanism of the voltage sensitivity of IRK1 inward-rectifier K+ channel block by the polyamine spermine. J Gen Physiol. 2005; 125(4):413–426. [PubMed: 15795311]
22. Pasternak, AP.; Shahipour, A.; Tang, H.; Teumelsan, NH.; Yang, L.; Walsh, SP. Preparation of piperazine derivatives for use as renal outer medullary potassium channel inhibitors. WO 2010129379. 2010.
23. For details on the MLPCN, see: http://mli.nih.gov/mli/mlpcn/
24. Davies NP, IMbrici D, Fialho D, Herd C, Bilsland LG, Weber A, Mueller R, Hitlon-Jones D, Ealing J, Boothman BR, Giunti P, Parsons LM, Thomas M, Manzur AY, Jurkat-Rott K, Lehmann-Horn F, Chinnery PF, Rose M, Kullman DM, Hanna MG. Andersen-Tawil syndrome: new potassium channel mutations and possible phenotypic variation. Neurology. 2005; 65(7):1083–1089. [PubMed: 16217063]
25. Schulze-Bahr E. Short QT Syndrome or Andersen Syndrome: Yin and Yang of Kir2.1 Channel Dysfunction. Circ Res. 2005; 96(7):703–704. [PubMed: 15831819]
26. Tristani-Firouzi M, Jensen JL, Donaldson MR, Sansone V, Meola G, Hahn A, Bendahhou S, Kwiecinski H, Fidzianska A, Plaster N, Fu YH, Ptacek LJ, Tawil R. Functional and clinical characterization of KCNJ2 mutations associated with LQT7 (Andersen syndrome). J Clin Invest. 2002; 110(3):381–388. [PubMed: 12163457]
27. Lin CW, Sim S, Ainsworth A, Okada M, Kelsh W, Lois C. Genetically increased cell-intrinsic excitability enhances neuronal integration into adult brain circuits. Neuron. 2010; 65(1):32–39. [PubMed: 20152111]
28. Yang CH, Rumpf S, Xiang Y, Gordon MD, Song W, Jan LY, Jan YN. Control of the postmating behavioral switch in Drosophila females by internal sensory neurons. Neuron. 2009; 61(4):519–526. [PubMed: 19249273]
29. For information on PubChem, please see: http://pubchem.ncbi.nlm.nih.gov/
30. Kennedy JP, Williams L, Bridges TM, Daniels RN, Weaver D, Lindsley CW. Application of combinatorial chemistry science on modern drug discovery. J Comb Chem. 2008; 10:345–354. [PubMed: 18220367]
31. For information of the Ricera Lead Profiling Screen see: http://www.ricerca.com/
32. Sackin H, Palmer LG, Krambis M. Potassium-dependent slow inactivation of Kir1.1 (ROMK) channels. Biophys J. 2004; 86(4):2145–2155. [PubMed: 15041655]
33. Tao X, Avalos JL, Chen J, MacKinnon R. Crystal structure of the eukaryotic strong inward-rectifier K+ channel Kir2.2 at 3.1 A resolution. Science. 2009; 326(5960):1668–1674. [PubMed: 20019282]
34. Dunbrack RL, Karplus M. Backbone-dependent Rotamer Library for Proteins Application to Side-chain Prediction. J Mol Biol. 1993; 230:543–574. [PubMed: 8464064]
35. Pettersen EF, Goddard TD, Huang CC, Couch GS, Greenblatt DM, Meng EC, Ferrin TE. UCSF Chimera - a visualization system for exploratory research and analysis. J Comput Chem. 2004; 13:1605–1612. [PubMed: 15264254]
36. Chang HK, Yeh SH, Shieh RC. The effects of spermine on the accessibility of residues in the M2 segment of Kir2.1 channels expressed in Xenopus oocytes. J Physiol. 2003; 553(Pt 1):101–112. [PubMed: 12963788]

37. Lu T, Nguyen B, Zhang X, Yang J. Architecture of a K+ channel inner pore revealed by stoichiometric covalent modification. Neuron. 1999; 22(3):571–580. [PubMed: 10197536]

38. Yi BA, Lin YF, Jan YN, Jan LY. Yeast screen for constitutively active mutant G protein-activated potassium channels. Neuron. 2001; 29(3):657–667. [PubMed: 11301025]

39. Tammaro P, Flanagan SE, Zadek B, Srinivansan S, Woodhead H, Hameed S, Klimes I, Hattersley AT, Ellard S, Ashcroft SM. A Kir6.2 mutation causing severe functional effects in vitro produces neonatal diabetes without the expected neurological complications. Diabetologia. 2008; 51(5): 802–810. [PubMed: 18335204]

40. Brideau C, Gunter B, Pikounis B, Liaw A. Improved statistical methods for hit selection in high-throughput screening. J Biomol Screen. 2003; 8:634–647. [PubMed: 14711389]

41. Kaibara M, Ishihara K, Doi Y, Hayashi H, Ehara T, Taniyama K. Identification of human Kir2.2 (KCNJ12) gene encoding functional inward rectifier potassium channel in both mammalian cells and Xenopus oocytes. FEBS Lett. 2002; 531:250–254. [PubMed: 12417321]

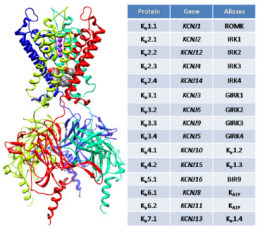

Protein	Gene	Aliases
$K_{ir}1.1$	*KCNJ1*	ROMK
$K_{ir}2.1$	*KCNJ2*	IRK1
$K_{ir}2.2$	*KCNJ12*	IRK2
$K_{ir}2.3$	*KCNJ4*	IRK3
$K_{ir}2.4$	*KCNJ14*	IRK4
$K_{ir}3.1$	*KCNJ3*	GIRK1
$K_{ir}3.2$	*KCNJ6*	GIRK2
$K_{ir}3.3$	*KCNJ9*	GIRK3
$K_{ir}3.4$	*KCNJ5*	GIRK4
$K_{ir}4.1$	*KCNJ10*	$K_{ir}1.2$
$K_{ir}4.2$	*KCNJ15*	$K_{ir}1.3$
$K_{ir}5.1$	*KCNJ16*	BIR9
$K_{ir}6.1$	*KCNJ8*	K_{ATP}
$K_{ir}6.2$	*KCNJ11*	K_{ATP}
$K_{ir}7.1$	*KCNJ13*	$K_{ir}1.4$

Figure 1.

Structural model of an inward rectifier potassium channel based on the $K_{ir}2.2$ crystal structure, highlighting the tetrameric structure. Each K_{ir} channel subunit possesses two membrane-spanning α-helical domains (M1 and M2) that are separated by an extracellular loop which forms the K^+ ion selectivity filter. The TMs then lead to the helix bundle crossing and the large cytoplasmic domain. Also shown is the K_{ir} family of ion channels highlighting both the gene and aliases commonly used in the literature.

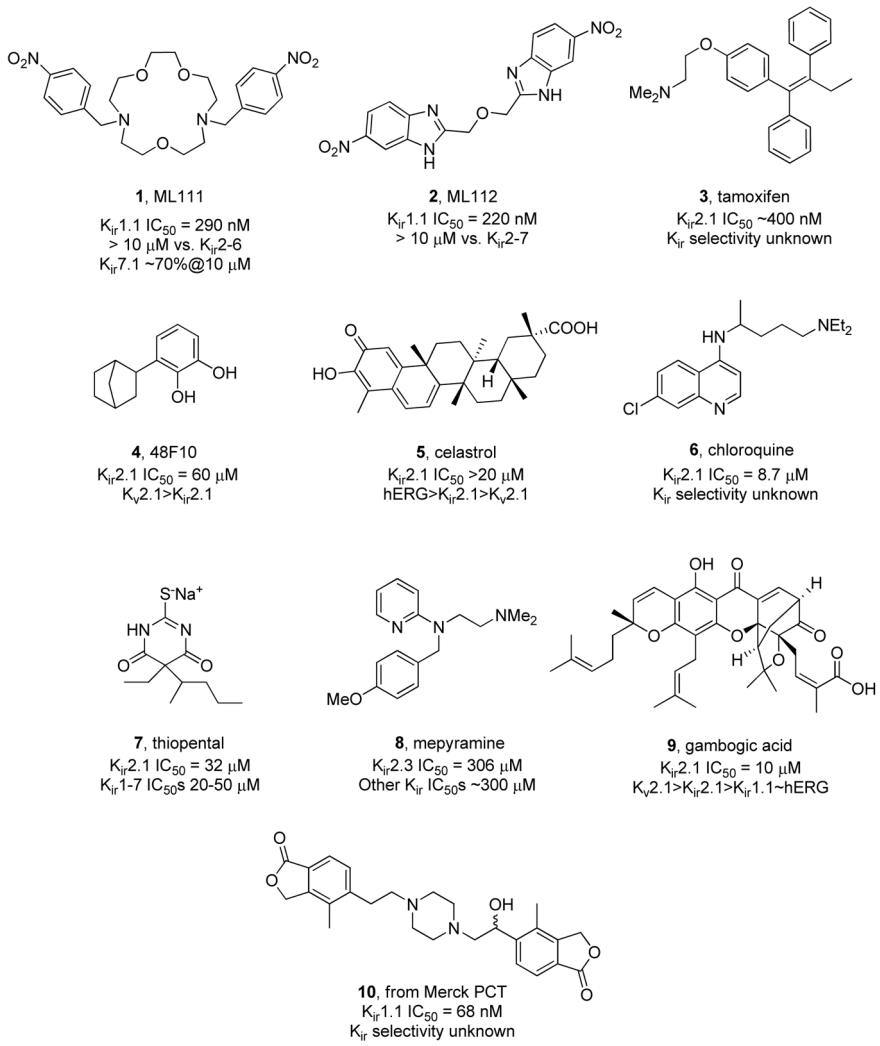

Figure 2.
Structures and activities of representative K_{ir} small molecule inhibitors.

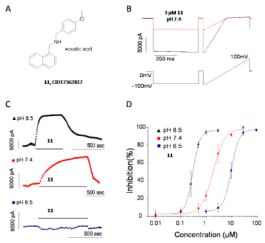

Figure 3.

Characterization of a novel $K_{ir}2.1$ inhibitor, **11**. A) Molecular structure of **11**. B) Representative traces for **11** inhibition of $K_{ir}2.1$ channel at 3μM. Current traces shown were recorded before (black trace) and after (red trace) applying 3μM **11** to the bath for 10 minutes. C) Representative time-course curve of $K_{ir}2.1$ inhibition by 3μM **11** at pH 8.5 (triangle), pH7.4 (circle), and pH6.5 (square). The time courses were representative results from 3–6 repeats. D) **11** dose-response curves for $K_{ir}2.1$ at pH 8.5 (triangle), pH 7.4 (circle) and pH6.5 (square). At pH 6.5, IC_{50} is 10.0 μM and Hill coefficient (N_H) is 1.8; at pH 7.4, IC_{50} is 1.9 μM and N_H is 1.7; at pH 8.5, IC_{50} is 290 nM and N_H is 4.0; n=6–12.

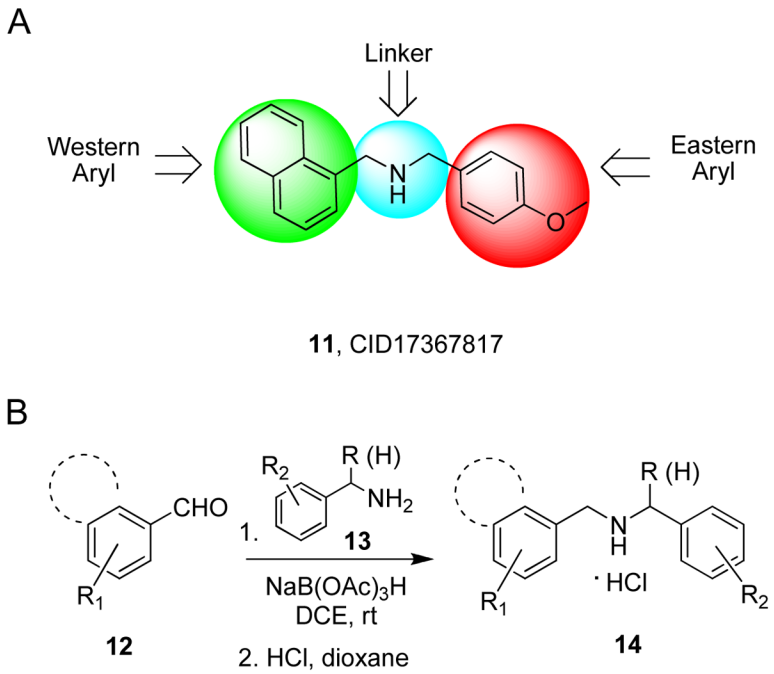

Figure 4.

Design and chemical lead optimization strategy for CID17367817, **11**/**ML133**. A) diversity-oriented modular approach to survey three regions of **11**; B) general synthetic approach employed for the iterative library synthesis of analogs **14**.

A

Cmpd	Structure	$K_{ir}2.1$ IC_{50} (nM)[a]
11	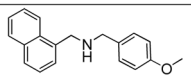	290
14a	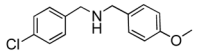	770
14b	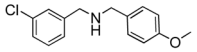	1,060
14c	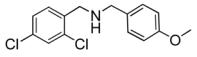	3,890
14d	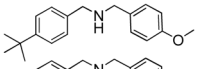	1,390
14e	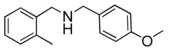	5,150
14f	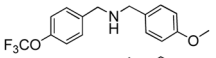	1,830
14g	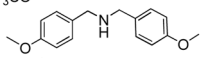	2,530
14h	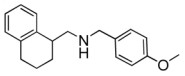	4,810
14i	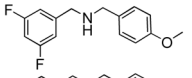	9,490
14j	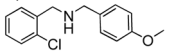	13,880
14k	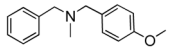	9,200 31,000[b]

[a]Manual patch clamp at pH 8.5 and average of at least three independent measurements. All compounds tested as the corresponding HCl salts. [b]Manual patch clamp at pH7.4

B

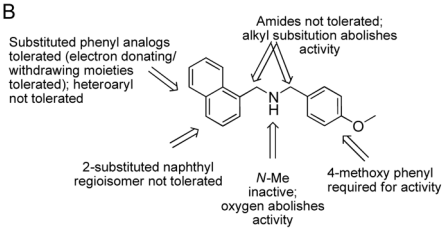

Figure 5.

SAR and lead optimization summary for CID17367817, **11**. A) SAR quickly established the necessity of the 4-OMebenzyl moiety, and all active analogs possessed this group; B) summary of observed SAR of over 50 analogs synthesized and evaluated examining all three regions of **11**.

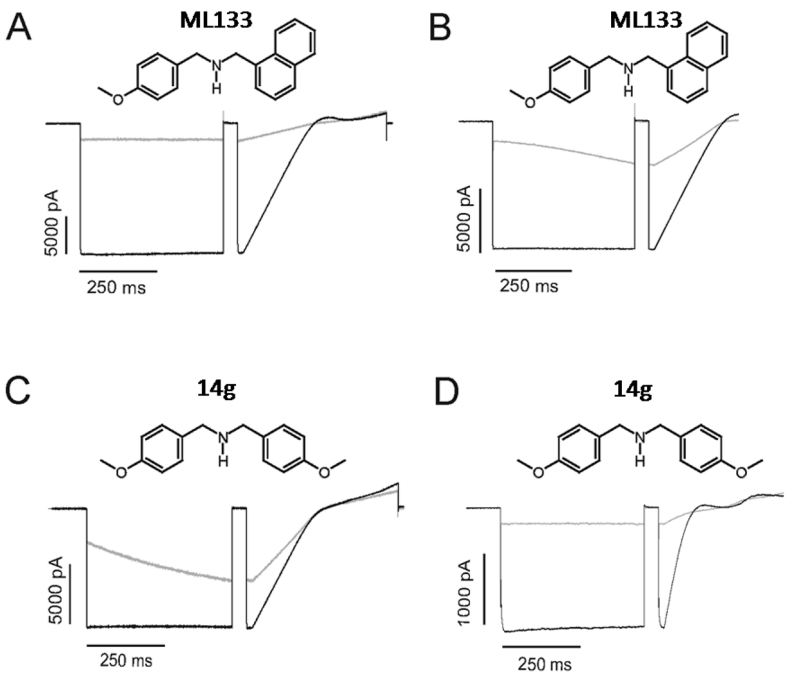

Figure 6.

ML133 blocked the ion conducting pathway of $K_{ir}2.1$ channel. A) 10 μM ML133 was not displaced by K^+ influx from the wild-type $K_{ir}2.1$. Cell was bathed in a pH 7.4 solution containing 140 mM K_o^+. B) K^+ influx (140 mM K_o^+) displaces 100 μM ML133 from the $K_{ir}2.1$ D172N/I176C mutant due to decreased compound affinity with channel. C) K^+ influx displaces compound 30 μM **14g** from the $K_{ir}2.1$ WT channel. D) Decrease of K_o^+ from 140 mM to 4 mM prevented 30 μM **14g** from being displaced from $K_{ir}2.1$ WT by K^+ influx. Note: Current traces shown above were recorded before (black trace) and after (grey trace) compounds (ML133 and **14g**) reached maximal inhibition at pH 7.4.

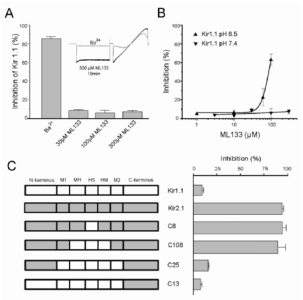

Figure 7.

Chimeric channels reveal critical domain(s) in $K_{ir}2.1$ mediating ML133 inhibition. A) $K_{ir}1.1$ is not sensitive to ML133 inhibition. 30μM, 100μM, or 300 μM ML133 did not inhibit $K_{ir}1.1$ (n=3–5). Inset: $K_{ir}1.1$ currents were not inhibited by 300 μM ML133 at pH 7.4 (black trace), while 5 mM Ba^{2+} completely inhibited $K_{ir}1.1$ (grey trace) B) ML133 dose-response curves for $K_{ir}1.1$ at pH 7.4 and pH 8.5. At pH 7.4, $K_{ir}1.1$ is not inhibited by up to 300 μM ML133. At pH 8.5, ML133 inhibited $K_{ir}1.1$ with IC_{50} of 85.5 μM. C) Chimeras between $K_{ir}1.1$ and $K_{ir}2.1$ exhibited differential sensitivity towards 30 μM ML133 at pH 7.4. Left panel: Chimeras were made by gradually displacing $K_{ir}2.1$ sequence by corresponding $K_{ir}1.1$ sequence as indicated. *N*-terminus: $K_{ir}2.1$ M1-L85; M1: $K_{ir}2.1$ V86-L109; MH: $K_{ir}2.1$ H110-T130; H5: $K_{ir}2.1$ A131-R148; HM: $K_{ir}2.1$ C149-A157; M2: $K_{ir}2.1$ V158-A181; C-terminus: $K_{ir}2.1$ K182-I428. Right panel: 30 μM ML133 inhibited over 80% of C8 and C108 current, but less than 20% of C25 and C13 currents.

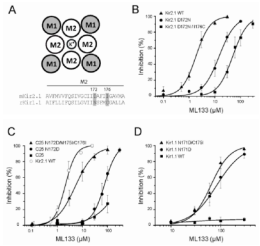

Figure 8.

Identification of the critical residuals for ML133 inhibition of $K_{ir}2.1$. A) Structural layout of $K_{ir}2.1$ transmembrane domains, and the sequence alignment of $K_{ir}2.1$ and $K_{ir}1.1$ inner transmembrane domain (M2). Non-conserved residues (e.g. Kir2.1 D172 and I176) facing the central cavity were highlighted in grey. B) $K_{ir}2.1$ N172D (IC_{50}=15.4 μM, N_H=1.3, circle) and $K_{ir}2.1$ N172D/I176C (IC_{50}=43.6μM, N_H=1.8, square) mutant is less sensitive to ML133 compared with $K_{ir}2.1$ WT (IC_{50}= 1.9μM, N_H=1.7, triangle) $K_{ir}2.1$ wild-type. C) ML133 dose-dependent block of C25 and its mutants at pH 7.4. C25 is slightly inhibited at 100 μM (square). C25 N172D is more sensitive to ML133 (IC_{50}=75.2μM, N_H=2.2, circle). C25 N172D/M175I/I176C restored high-affinity ML133 block (IC_{50}=5.8μM, N_H=1.1, triangle). K_{ir} 2.1 wild-type IC_{50}=1.9μM (N_H=1.7, grey hollow circle).D. $K_{ir}1.1$ N171D (IC_{50}=83.6 μM, N_H=1.6, circle) and $K_{ir}1.1$ N171D/C175I (IC_{50}=64.0μM, N_H=2.3, triangle) partially restored sensitivity to ML133 compared with $K_{ir}1.1$ (square).

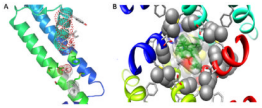

Figure 9.
Crystal structure of $K_{ir}2.2$ and our $K_{ir}2.1$ homology model. A) View of $K_{ir}2.2$ TM2 where ML133 is proposed to bind in $K_{ir}2.1$. B) Kir2.1 homology model based on crystal structure of $K_{ir}2.2$ with ML133 docked based on mutagenesis studies.

Table 1

The selectivity of ML133 inhibition and $K_{ir}2.1$ D172/I176 motif

Channel	Sequence alignment of M2 transmembrane domain																									IC$_{50}$ (μM) pH 7.4
																172				176						
mKir2.1	A	V	F	M	V	V	F	Q	S	I	V	G	C	I	I	D	A	F	I	I	G	A	V	M	A	1.9
rKir1.1	A	I	F	L	L	I	F	Q	S	I	L	G	V	I	I	N	S	F	M	C	G	A	L	L	A	>300
hKir2.2	A	I	F	M	V	V	A	Q	S	I	V	G	C	I	I	D	S	F	M	I	G	A	I	M	A	2.9
hKir2.3	A	V	I	A	V	V	V	Q	S	I	V	G	C	V	I	D	S	F	M	I	G	T	I	M	A	4.0
hKir2.6	A	V	F	M	V	V	A	Q	S	I	V	G	C	I	I	D	S	F	M	I	G	A	I	M	A	2.8
rKir4.1	A	I	E	L	L	I	A	Q	L	V	L	T	T	I	L	E	I	F	I	T	G	T	F	L	A	76.0
rKir6.2	A	I	L	I	L	I	V	Q	N	I	V	G	L	M	L	N	A	I	M	L	G	C	I	F	M	7.7
hKir7.1	A	I	A	L	L	A	I	Q	N	L	L	G	L	M	L	E	A	F	I	T	G	A	F	V	A	32.9